Surface & Coatings Technology 205 (2011) 3905–3908

Contents lists available at ScienceDirect

Surface & Coatings Technology

journal homepage: www.elsevier.com/locate/surfcoat

Fabrication and photophysical properties of singlet oxygen generating nanoporous membrane☆

Kang-Kyun Wang, Min-Su Jung, Kyong-Hoon Choi, Hee-Won Shin, Seung-Im Oh, Ji-Eun Im, Da-Hee Kim, Yong-Rok Kim *

Department of Chemistry, Yonsei University, Shinchon-Dong 134, Seodaemun-Gu, Seoul, 120-749, Republic of Korea

ARTICLE INFO

Available online 20 August 2010

Keywords:
Singlet oxygen
Nanoporous alumina membrane
Photosensitizer

ABSTRACT

The nanoporous alumina membranes (NAMs) were fabricated by a two-step aluminium anodic oxidation process. The fabricated NAMs have controllable pore diameters (40–80 nm) and unidirectionally ordered pore direction. The surface of the NAM was modified with the organo-silane agent (APTES: (aminopropyl) triethoxysilane) to induce ionic bonding between the NAM and the photosensitizer (TSPP: tetrakis(p-sulfonatophenyl)porphyrin). The morphology and chemical nature of the surface modified NAM were studied by field emission scanning electron microscope (FE-SEM), FT-IR spectra, and thermo gravimetric analysis (TGA). Furthermore, this singlet oxygen generating nanoporous membranes (SGNMs) were investigated, in detail, to understand their photophysical properties and the singlet oxygen generation efficiency which were the essential factors for their applications. Steady-state spectroscopies and nanosecond laser induced time-resolved spectroscopy were applied to get information on all photophysical properties including the lifetime of singlet oxygen which depended on the pore diameter of the SGNM.

1. Introduction

Singlet oxygen, $O_2(^1\triangle_g)$, has been a subject for a long time in chemical and biological fields due to its reactivity and selectivity to the system. It has many applications such as photodynamic cancer therapy, decontamination of blood product, water disinfectant, DNA programed, degradation of undesired organic compounds, and stereo-selective synthesis of organic materials [1–6].

Singlet oxygen generation with mesoporous materials has been demonstrated with zeolite and MCM-41 functionalized with photo-sensitizers [7]. From the fixation of photosensitizers to zeolites or MCM-41, thermal stability and handling advantage could be achieved. However both porous materials have a powder like property and a few nanometers of very small pore diameter which disturb the good contact between the singlet oxygen and the target system [8].

In this work, we report a new fabrication of the singlet oxygen generating nanoporous membrane (SGNM) and its photophysical properties. First, nanoporous alumina membranes were fabricated by a two-step aluminum anodic oxidation process [9]. Then the surface of the fabricated NAMs was modified with organo-silane agent [10–12]. Finally, TSPP molecules were ionically bonded to ammonium-terminated NAMs surface by a dipole–dipole interaction [13]. Generated singlet oxygen from the fabricated SGNMs was directly monitored with the nanosecond laser induced time-resolved spectroscopic method.

2. Experimental details

2.1. Preparation of singlet oxygen generating nanoporous membranes (SGNMs)

The overall synthetic procedure of the SGNM is shown in Scheme 1. The commercially available photosensitizer (TSPP: tetrakis(p-sulfonatophenyl)porphyrin) used in this experiment was purchased from Fluka (98.0%). The nanoporous alumina membranes (NAMs) were prepared by a two-step anodizaton. Details of the preparation were described in Reference [9]. For the surface modification of NAMs, NAMs were immersed into the hydroperoxide solution in order to enhance the hydroxyl group on the NAMs' surface. Then NAMs were reacted with the APTES ((aminopropyl) triethoxysilane, 0.1 M)/$CHCl_3$ solution at room temperature for 1 h. APTES was covalently bonded to the nanoporous alumina membrane by silanisation reaction between the hydroxyl group on the surface of the nanoporous alumina membrane and the ethoxy group of the APTES [10–12]. After washing and drying, the surface modified NAMs were immersed in TSPP(10^{-5} M)/water solution at an acid condition (pH 5) for 1 h and then washed with distilled water [13].

☆ This paper was presented at the AEPSE 2009 conference.

* Corresponding author. Tel.: +82 2 2123 2646; fax: +82 2 364 7050.
E-mail address: yrkim@yonsei.ac.kr (Y.-R. Kim).

0257-8972/$ – see front matter © 2010 Elsevier B.V. All rights reserved.
doi:10.1016/j.surfcoat.2010.08.061

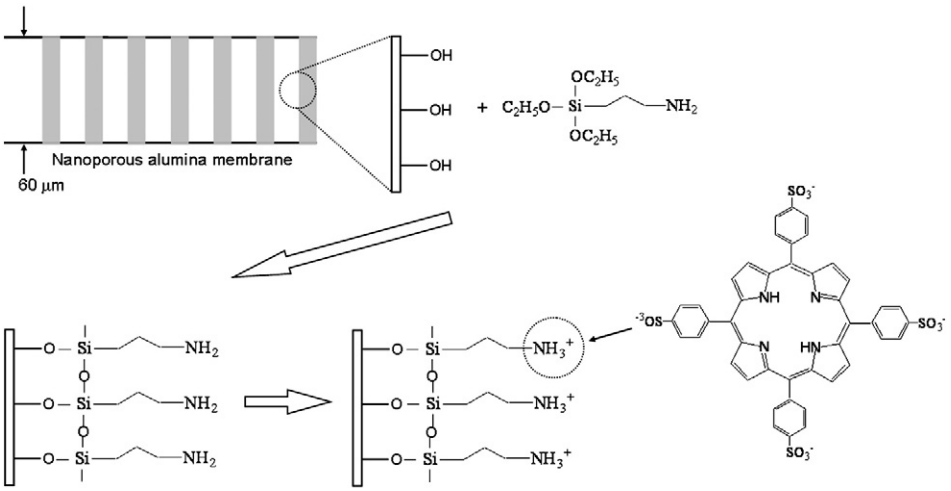

Scheme 1. Preparation of the singlet oxygen generating nanoporous membrane.

2.2. Characterization of singlet oxygen generating nanoporous membranes (SGNMs)

Surface morphologies of NAMs were observed by field emission scanning electron microscopy (FE-SEM, JEOL, 6500F). The surface of the modified NAM was confirmed by FT-IR spectra (Nicolet, impact 400), and thermogravimetric analysis (TGA, TA instrument, TA 2050). Steady-state absorption and fluorescence spectra were obtained by using a UV–Vis spectrophotometer (Shimadzu, UV-160A) and a spectrofluorimeter (Hitachi, F-4500), respectively. For the membrane sample, diffuse reflectance spectra were recorded by a UV–Vis spectrophotometer (Jasco, V-550) equipped with an integrating sphere (Jasco, ISV-469).

2.3. Detection of singlet oxygen

A Nd-YAG laser (BMI series, 7 ns FWHM pulse) pumped optical parametric oscillator (OPO) laser (B.M. Industries OP901-355, 5 ns FWHM pulse) was utilized as an excitation source for the detection of time-resolved singlet oxygen phosphorescence. Phosphorescence signal was collected at a perpendicular angle to the excitation beam and detected with germanium photodiode (EG&G, Judson) after passing through a set of cut-off (<1000 nm, CVI) and interference filters (1270 nm, spectrogon). The signal was acquired by 500 MHz digital oscilloscope (Hewlett Packard, 54520A) and transferred to a computer for data analysis [14,15].

3. Results and discussion

SEM images of the fabricated pure NAMs are shown in Fig. 1. The fabricated pore diameters of nanochannels are controlled to be 40 and 80 nm by changing the electrolytes and the applied voltages: 0.3 M sulfuric acid at 25 V for the pore diameter of 40 nm, and 0.3 M oxalic acid at 40 V for the 80 nm diameter. The thickness of the NAMs is maintained to be 60 μm for the different oxidation conditions for 10 h at the sulfuric acid and 5 h at the oxalic acid. The NAMs are fabricated as free standing films [9].

Surface modification of NAMs with hydrophobic silane, APTES, is confirmed with the ATR-IR spectra. Fig. 2 shows the ATR-IR spectra of the APTES, the NAM, and the APTES bounded NAM. The spectrum of APTES is assigned to be the $-CH_3$ symmetric vibration mode at the 2973 cm^{-1} and $-CH_2$ symmetric and asymmetric vibration modes at 2879 and 2924 cm^{-1}, respectively, from References [10,16,17]. The spectrum of the NAM shows –OH stretching vibration modes at 3400 cm^{-1} [10,11]. In the spectrum of the APTES bounded NAM, the peaks of the $-CH_2$ symmetric (2879 cm^{-1}) and asymmetric vibration modes (2924 cm^{-1}) remain. On the other hand, the $-CH_3$ (2973 cm^{-1}) vibration peak disappears significantly in its intensity. It is due to the removal step of the methyl group ($-CH_3$) of APTES during the attachment reaction process of APTES and NAM [17,18]. The increased peak intensity of the –OH (3650–3200 cm^{-1}) stretching vibration implies that the hydroxyl group of the NAM surface is enhanced throughout the surface modification process. Therefore, the result confirms that the APTES is attached to the NAM surface by the

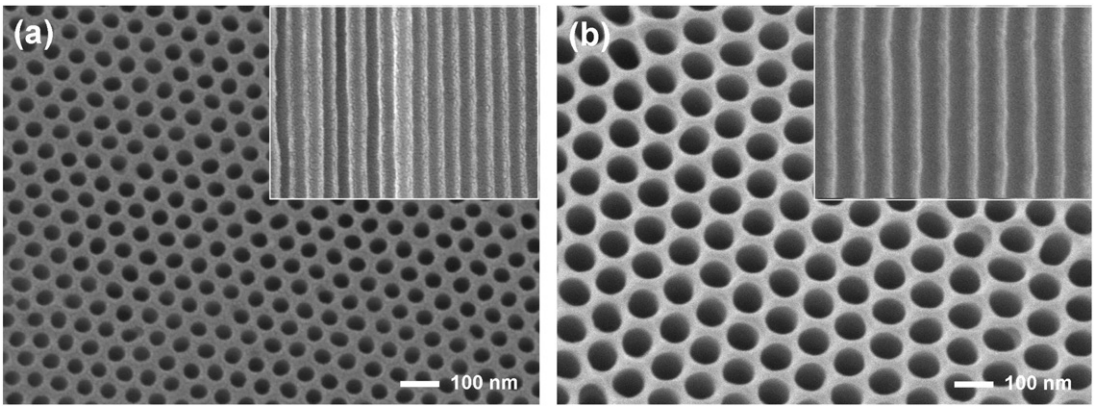

Fig. 1. FE-SEM images of the nanoporous alumina membrane with pore diameters of (a) 40 and (b) 80 nm. The insets present the cross-section views.

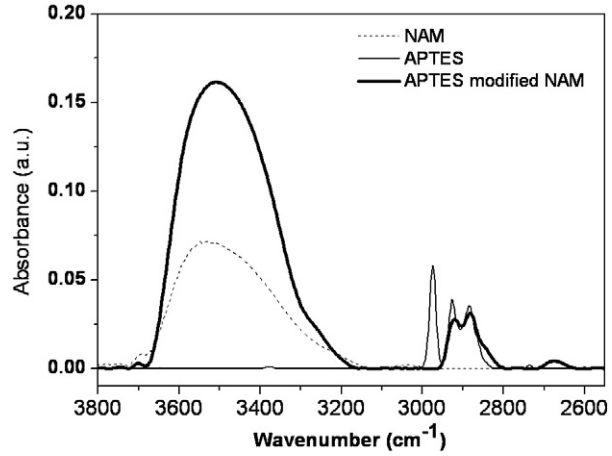

Fig. 2. ATR-IR spectra of the pure NAM (dashed line), the pure APTES (thin solid line) and the surface modified NAM with APTES (thick solid line).

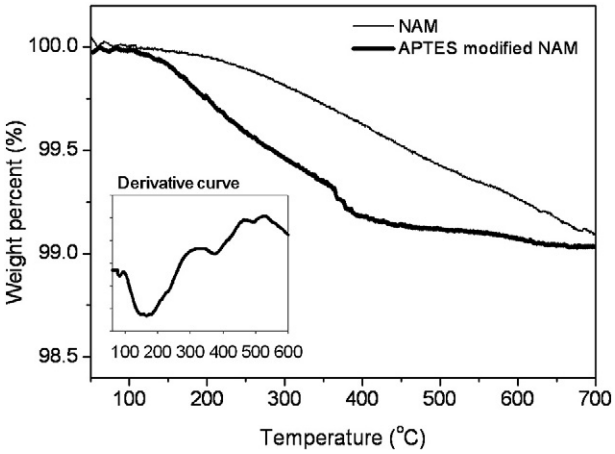

Fig. 3. Thermogravimetric data of the pure NAM (thin solid line) and the APTES bonded to NAM (thick solid line). The inset presents the derivative curves of the surface modified NAM with APTES.

silanisation reaction between the hydroxyl group of the NAM and the ethoxy group of the APTES.

Supplemental information on the formation of the functional groups on the NAM surface is obtained from TGA measurement. As shown in Fig. 3, the pure NAM shows a weight loss of 0.01% at the temperature range of 50–200 °C. It is considered to be due to the loss of physically absorbed water on the surface. The APTES coupled to the NAM experiences the first loss that is the same decomposition step as the pure and the second weight loss at a higher temperature range of 300–400 °C. The second weight loss is responsible for the loss of the aminopropyl groups coupled on the surface of the functionalized NAM [18,19].

Diffuse reflectance UV–Vis absorption spectrum of the SGNM is presented in Fig. 4a with the comparison of the absorption spectrum of the pure TSPP molecules in an aqueous solution. The absorption spectrum of the TSPP bounded NAM was obtained by using diffuse reflectance spectrophotometer due to big scatterings from the membrane. Diffuse reflectance spectrum is a type of the absorption spectrum measured by the scattering from the surface of the sample. This diffuse reflectance spectrum is translated into the absorption spectra by the Kubelka–Munk method as follows:

$$\frac{K}{S} = \frac{(1-R)^2}{2R}$$

where K indicates the absorption coefficient, and S and R represent the scattering coefficient and the absolute reflectance, respectively [20]. The spectrum of TSPP shows one B band (413 nm) and four Q bands (516, 553, 580, and 634 nm) [21]. The diffuse reflectance absorption spectrum of the SGNM also includes the B and Q bands at similar wavelengths but with broader shapes and red shifted peak positions. Such difference in the peak width and position is possibly due to the self-coupling of TSPPs attached on the surface and the inhomogeneous bonding nature of TSPP to the surface of the SGNM. The chemical bonding site is to depend on the non-uniform bonding sites on the SGNM surface that mostly consists of the inner surface of the channels, which causes the inhomogeneity of the peak broadening. The red shifted peaks are attributed to the intermolecular coupling of the TSPP molecules bonded to the surface of the SGNM. Since the bonded molecules experience much less degrees of freedom, they have higher possibility to be coupled together compared with the free molecules of TSPP (8.2×10^{-5} M) in an aqueous solution [22,23]. The difference in the absorption spectra also appeared in the emission spectra representing the excited states of TSPP for the same reasons (Fig. 4b).

The most critical factor for the proof of the singlet oxygen generation from the SGNM ought to be the direct detection of phosphorescence from the singlet oxygen molecules generated from the photoexcited TSPP bonded to the surface of the NAM. The measured phosphorescence signals are presented in Fig. 5. The decays are fitted to a single exponential function, resulting to the lifetimes of the singlet oxygen

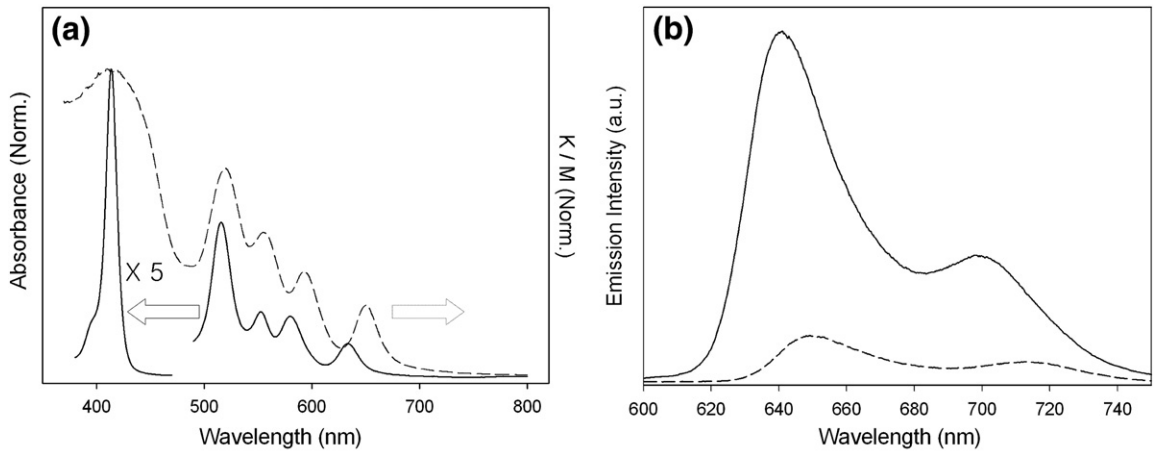

Fig. 4. (a) Absorption and (b) emission spectra of the pure TSPP (8.2×10^{-5} M) in an aqueous solution (solid line) and the TSPP bonded NAM (dashed line). The absorption spectrum of the TSPP bonded NAM is obtained by applying the Kubelka–Munk function to the diffuse reflectance spectrum. The excitation wavelength is 515 nm for the emission spectrum.

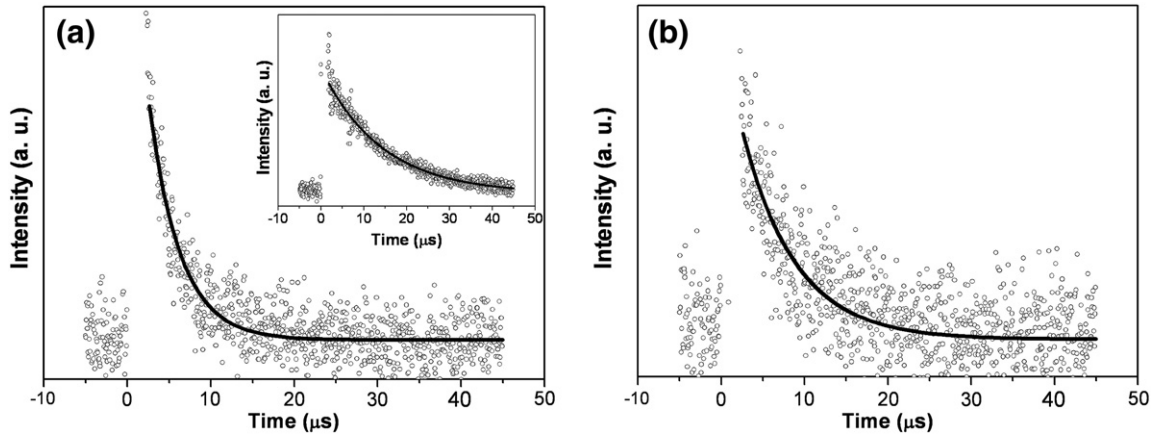

Fig. 5. Phosphorescence decay of the singlet oxygen from SGNMs with pore diameters of (a) 40 and (b) 80 nm detected at 1270 nm in ethanol. The inset presents the singlet oxygen phosphorescence signals from the pure TSPP molecules in ethanol.

depending on the environmental condition [14]. The singlet oxygen lifetime of the pure TSPP molecules in ethanol solution is measured to be ~14 μs that is a characteristic relaxation time of singlet oxygen in an ethanol solvent [24]. However, the singlet oxygen lifetimes from the SGNMs with pore diameters of 40 and 80 nm are 3.7 and 6.4 μs, respectively. Assuming a typical diffusion coefficient for oxygen to be 1.31×10^{-9} m^2 s^{-1} of D, the average distance that the singlet oxygen can diffuse in ethanol is estimated to be approximately 190 nm during 14 μs of the lifetime from the root-mean-square linear displacement of $(2Dt)^{1/2}$ [25]. The faster lifetimes of 3.7 and 6.4 μs measured from the SGNMs correspond to 141 and 185 nm with the same estimation process, respectively. From the expected diffusion distances of 141 and 185 nm, the singlet oxygen generated from the inside of the nanochannels of the NAM will experience the serious collisional quenching dynamics with the silicate inner surface of the nanochannels of 40 and 80 nm in their diameters. Furthermore, the faster lifetime of 3.7 μs for the 40 nm diameter channels than the 6.4 μs for the 80 nm diameter channels also supports the collisional quenching phenomena of singlet oxygen to the inner surface of the nanochannels within the SGNM. Such dependence of $^1O_2$ lifetime on the pore diameters indicates that most TSPP are bonded inside the surface of the nanochannels of the NAM. In order to further clarify the point, the surface area ratio of the outer surface and the total surface including the inside surface area is calculated for a nanoporous membrane (domain size of $8\times30\times0.06$ mm^3 and pore diameter of 80 nm). The estimated area ratio is 6.7×10^{-4}, implying that TSPP can couple to the inside surface of nanochannels of the SGNM approximately 10,000 times more than the outer surface. Therefore, it should result to the faster lifetime of $^1O_2$ for the SGNM with smaller pore diameter of the nanochannels since most of the $^1O_2$ generated react with the OH groups attached inside the channel of the membrane.

4. Conclusions

It has successfully been demonstrated that the singlet oxygen of highly oxidative species is being generated from SGNMs which are fabricated through the surface modification of NAM with organo-silane agents, APTES, and the photosensitizer of TSPP. Singlet oxygen dynamics depending on the pore diameters of the nanochannels of SGNM is also investigated to provide the effective activity within the nanochannels as an oxidant. Therefore, based on the experimental observations, the new singlet oxygen generating nanoporous membrane may have a high potential for the applications of the size-exclusive destruction membrane for harmful biological and environmental poisons as well as the catalytic membrane for size selective photocatalytic reactions.

Acknowledgment

This study was supported by a grant from the Korea Healthcare Technology R&D Project, Ministry for Health, Welfare and Family Affairs, Republic of Korea (A085136).

References

[1] K. Kalka, H. Merk, H. Mukhtar, J. Am. Acad. Dermatol. 42 (2000) 389.
[2] T.W. Steief, Med. Hypothesis 60 (2003) 567.
[3] R. Bonnetta, M.A. Krystevab, I.G. Lalovb, S.V. Artarsky, Water Res. 40 (2006) 1269.
[4] E. Clo, J.W. Snyder, N.V. Voigt, P.R. Ogilby, K.V. Gothelf, J. Am. Chem. Soc. 128 (2006) 4200.
[5] L. Villén, F. Manjŏn, D.G. Fresnadillo, G. Orellana, Appl. Catal. B 69 (2006) 1.
[6] S.N. Patil, Fei Liu, Org. Lett. 9 (2007) 195.
[7] C.J. Liu, S.G. Li, W.Q. Pang, C.M. Che, Chem. Commun. (1997) 65.
[8] W.S. Chea, S.W. Lee, S.J. Im, S.W. Moon, W.C. Zin, J.K. Lee, Y.R. Kim, Chem. Commun. (2004) 2554.
[9] H. Masuda, M. Satoh, Jpn. J. Appl. Phys. 35 (1996) L126.
[10] A.M.M. Jani, J. Zhou, M.R. Nussio, D. Losie, J.G. Shapter, N.H. Voelcker, Proc. of SPIE 7267 (2008) 0T01.
[11] V. Szczepanski, I. Vlassiouk, S. Smirnov, J. Mem. Sci. 281 (2006) 587.
[12] I. Vlassiouk, A. Krasnoslobodtsev, S. Smirnov, M. Germann, Langmuir 20 (2004) 9913.
[13] W. Xu, H. Guo, Daniel L. Akins, J. Phys. Chem. B 105 (2001) 1543.
[14] J.H. Ha, S. Ko, C.H. Lee, W.Y. Lee, Y.R. Kim, Chem. Phys. Lett. 34 (2001) 271.
[15] J.S. Kim, H.J. Yoon, S.H. Kim, K.K. Wang, T. Ishii, Y.R. Kim, W.D. Jang, J. Mater. Chem. 19 (2009) 4827.
[16] X.S. Zhao, G.Q. Lu, A.K. Whittaker, G.J. Millar, H.Y. Zhu, J. Phys. Chem. B 101 (1997) 6525.
[17] V.K.S. Hsiao, J.R. Waldeisen, Y. Zheng, P.F. Lloyd, T.J. Bunningb, T.J. Huang, J. Mater. Chem. 17 (2007) 4896.
[18] K. Ishibashi, K. Tanaka, A.H. Iwata, K. Miyamoto, Y. Kimura, M. Niwano, J. Appl. Phys. 47 (2008) 3204.
[19] M. Charrerjee, T. Iwasaki, H.Y. Hayashi, Y. Onodera, T. Ebina, T. Nagase, Catal. Lett. 52 (1998) 21.
[20] P. Kubelka, F. Munk, Z. Tech, Phys. 12 (1931) 593.
[21] M. Pineiro, M.M. Pereira, G. Rocha, A.M. D'A, L.G. Arnaut, S. Formosinho, J. Photochem. Photobiol. A Chem. 138 (2001) 147.
[22] B.T. Holland, C. Walkup, A. Stein, J. Phys. Chem. B 102 (1998) 4301.
[23] S. Subbiah, R. Mokaya, Chem. Commun. (2003) 860.
[24] P.B. Merkel, R. Nilson, D.R. Kearns, J. Am. Soc. 94 (1972) 1030.
[25] M. Okamoto, J. Photochem. Photobiol. A Chem. 162 (2004) 17.